

BOLD susceptibility map reconstruction from fMRI by 3D total variation regularization

Z. chen¹, A. Caprihan¹, and V. Calhoun^{1,2}

¹Mind Research Network, Albuquerque, NM, United States, ²Electrical and Computer Engineering, University of New Mexico, Albuquerque, NM, United States

Introduction: BOLD activity disturbs the blood magnetic susceptibility distribution through variations in paramagnetic oxyhemoglobin and diamagnetic deoxyhemoglobin, which can be depicted by a 3D susceptibility map $\Delta\chi(x,y,z)$. In BOLD fMRI, the blood magnetization under a main magnetic field B_0 establish a BOLD-induced magnetic field $\Delta B(x,y,z)$ which can be detected and presented in forms of a complex-valued image $C(x,y,z)=A(x,y,z)\exp(-i\Phi(x,y,z))$. The goal of brain fMRI is to depict the BOLD activity in terms of $\Delta\chi(x,y,z)$ from $C(x,y,z)$, which is a 3D inverse problem. In this work, we report a solution by the split Bregman¹ algorithm of total variation (TV) regularization. Numerical simulation and phantom experiment are presented.

Methods: Suppose the BOLD activity causes a 3D biomagnetic susceptibility disturbance $\Delta\chi(x,y,z)$, which establishes a magnetic field disturbance distribution $\Delta B(x,y,z)$ by a 3D convolution $\Delta B(x,y,z)=\Delta\chi(x,y,z)*h(x,y,z)+noise(x,y,z)$ during MRI scanning, with $h(x,y,z)=[3z^2/(x^2+y^2+z^2)-1]/[4\pi\epsilon_0(x^2+y^2+z^2)^{3/2}]$. Through intravoxel spin procession dephasing, the BOLD fMRI produces a 3D complex image $C(x,y,z)=A(x,y,z)\exp(-i\Phi(x,y,z))$. From the phase component $\Phi(x,y,z)$, we can calculate the BOLD-induced magnetic field by $\Delta B(x,y,z)=-\Phi(x,y,z)/\gamma TE$, where γ is the gyromagnetic ratio and TE the echo time. In principle, the 3D inverse problem for the noisy convolved image $\Delta B(x,y,z)$ can be solved by filter truncation in the Fourier domain^{2,3}, which involves a truncation approximation for removing poles in the inverse filter. Alternatively, we herein suggest the use of the split Bregman¹ total variation algorithm for finding $\Delta\chi(x,y,z)$ from $\Delta B(x,y,z)$ with the kernel $h(x,y,z)$ in the presence of Gaussian noise. The Bregman TV algorithm is a 3-subproblem minimization procedure, as expressed by¹

$$\bar{u} = \arg \min_{d,v,u} \iiint |\bar{d}| dV + \frac{\lambda}{2} \iiint (h * \Delta\chi - \Delta B)^2 dV + \frac{\gamma_1}{2} \|d - \nabla u - \bar{b}_1\|_2^2 + \frac{\gamma_2}{2} \|v - h * u - \bar{b}_2\|_2^2, \text{ with } d = \nabla u, v = h * u$$

where $\{b_1, b_2\}$ are variables related to the split Bregman iteration algorithm, and $\{\lambda, \gamma_1, \gamma_2\}$ denote the regularization parameters. We demonstrate this algorithm with numerical simulation and phantom dataset. In our numerical simulation, we predefine a $\Delta\chi(x,y,z)$ by a $128 \times 128 \times 128$ matrix containing a cylinder convolved with $h(x,y,z)$ and including additive Gaussian noise. The 3D inverse problem is solved by both the filter-truncated Fourier transform and Bregman TV algorithms. In the phantom experiment, a plastic tube is filled with gadolinium and scanned with an EPI sequence.

Results and Discussion. Figure 1 shows the numerical simulation results, in which the predefined $\Delta\chi(x,y,z)$ in (a) containing a cylinder is the exact input for the Bregman TV algorithm. After convolving with $h(x,y,z)$ and adding Gaussian noise (noise level =0.05), as displayed in (b), we find the 3D inverse solution by filter-truncation Fourier transform in (c) and by the Bregman TV algorithm in (d). The profiles of a scanline along $\Delta\chi(x,0,0)$ in (a)(c)(d) are plotted in (e) for quantitative comparison. It is seen that the Bregman TV algorithm produces a better 3D inverse solution from the blurred and noisy volume. Due to infinite poles associated with 3D inverse filter and noise, the filter-truncated Fourier transform algorithm incurs not only artifacts but also an energy shift (due to removal of the 3D filter poles by a threshold truncation).

Using an EPI-complex sequence, we conducted phantom experiments. The phantom is a plastic tube filled with diluted Gd (dilution=0.4mL/30mL). The tube was immersed in a water container and posed in a vertical orientation with respect to B_0 during MRI scanning. The magnetic susceptibility map was reconstructed by the Bregman TV algorithm and was provided in Fig. 2, the field map was calculated from the phase components of two EPI complex images (at two TEs). Bothe the inverse solutions from the filter-truncation method and TV iteration methods are provided. It is seen that the flat distributions at the sagittal and axial sections of the Gd-filled tube can be better reconstructed by the TV iteration than by the truncated Fourier filtering method. It is also observed in Fig. 2 that the reconstructed magnetic susceptibility map from BOLD phase image is different from the BOLD magnitude image: the susceptibility map at the cross section of the cylinder is flat whereas the magnitude pattern bears a central dip and edge enhancement. We may understand the difference between the BOLD magnitude image and reconstructed susceptibility map from the fact: the former is due to dynamic (dependent upon TE) nonlinear intravoxel dephasing mechanism; however, the later is in principle invariant to TE for the static phantom experiment.

Conclusion: It is an ill-posed inverse problem to find the BOLD activity map from a complex-valued image acquired by BOLD fMRI. The split Bregman total variation iterative regularization can reconstruct the susceptibility map better than the truncated Fourier filtering method. A phantom experiment shows that the reconstructed susceptibility map bears differences from the magnitude component of the EPI complex image. However, the magnitude map of the EPI complex image may approximate the magnetic susceptibility map to a great extent.

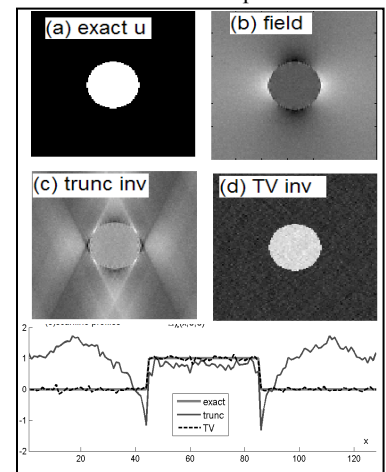


Fig.1 numerical simulation.

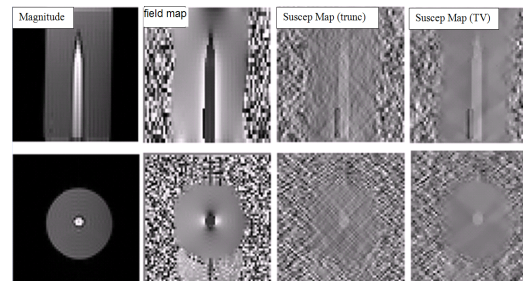


Fig.2 Gd-tube experiment (top row: sagittal plane, bottom row: axial plane)

References: [1]T. Goldstein and S. Osher, The Split Bregman Algorithm for L1 Regularized Problems, SIAM J. Imaging Sci., 2 (2009), pp. 323{343. 2.[2]. Wharton S. et al, MRM 63:1292-04 (2010). 3. Olafsson V. et al IEEE TMI 27 :9, 1177-88 (2008).